Energy band structure and optical response function of icosahedral $B_{12}As_2$: A spectroscopic ellipsometry and first-principles calculational study

S. Bakalova,[1] Y. Gong,[1] C. Cobet,[2] N. Esser,[2] Y. Zhang,[3] J. H. Edgar,[3] Y. Zhang,[4] M. Dudley,[4] and M. Kuball[1]
[1]*H.H. Wills Physics Laboratory, University of Bristol, Bristol BS8 1TL, United Kingdom*
[2]*Institute for Analytical Sciences (ISAS), Berlin, Germany*
[3]*Department of Chemical Engineering, Kansas State University, Manhattan, Kansas 66506, USA*
[4]*Department of Materials Science and Engineering, SUNY, Stony Brook, New York 11794, USA*
(Received 26 November 2009; revised manuscript received 13 January 2010; published 19 February 2010)

An experimental and theoretical study on the dielectric-response function of icosahedral $B_{12}As_2$ in the spectral region between 1.24 and 9.8 eV is presented. Comprehensive experimental information on the energy band structure from the analysis of features in the optical dispersion was complemented by spin-orbit first-principles calculations. The lowest indirect band gap width is 3.2 eV; the two lowest direct interband transitions are at 3.46 and 3.9 eV. High-energy critical points are assigned to specific electron transitions in the Brillouin zone and their dimensionality was determined. The static dielectric constant of $B_{12}As_2$ is uniaxially anisotropic with values of 7.84 and 9.02 for polarization perpendicular and parallel to the trigonal axis. Hole and electron effective masses are derived from the band dispersions.

DOI: 10.1103/PhysRevB.81.075114 PACS number(s): 71.20.Nr, 78.20.Ci, 78.40.Fy

I. INTRODUCTION

$B_{12}As_2$ with its exceptional radiation hardness, high melting temperature, and excellent mechanical properties is of great interest for applications under extreme conditions, such as beta-voltaic cells and neutron detectors. Recent progress in material growth[1] has made feasible the first working $B_{12}As_2$-based devices, such as *pn* junction diodes.[2] Despite this progress little is known about the fundamental properties of this new material, even on its electronic band structure that determines the underlying physics of transport and optical properties.

The basic structural unit of $B_{12}As_2$ are B_{12} icosahedra with metalliclike three-center internal bonds, common for the class of boron-rich solids. In $B_{12}As_2$, boron icosahedra occupy the vertices of a rhombohedral unit cell with the As-As chains along the trigonal axis[3] (Fig. 1). Several theoretical studies have been published on the calculation of the electronic structure of icosahedral borides, including also $B_{12}As_2$, for which the band gap was reported as indirect in the range of 2.3–2.78 eV.[5–8] Spin-orbit effects owing to the heavy As atoms were not considered in these reports. There has been no detailed experimental report on the electronic band structure of $B_{12}As_2$ for evaluating these theoretical studies. To our best knowledge, the only experimental information on $B_{12}As_2$ band structure are optical-absorption spectra reported by Slack *et al.*[9] from which an indirect band gap of 3.47 eV was derived.

In this work, we report spectroscopic ellipsometry results on icosahedral $B_{12}As_2$ films in the photon energy range from the near infrared (1.24 eV) to the vacuum ultraviolet (9.8 eV). First-principles calculations were performed to complement the experimental data. Spin-orbit interaction was considered by fully relativistic approach. The experimental critical points (CPs) and their line shape are compared to the theoretical optical response, identifying important features of the band structure of $B_{12}As_2$, such as the fundamental band edge and high-energy electron transitions.

The paper is organized as follows. Section II presents experimental details of the $B_{12}As_2$ samples growth, ellipsometry measurements, and derivation of the experimental optical response function. Section III presents the computational approach for first-principles analysis of the band structure and theoretical optical response. Section IV consist of experimental results on dielectric function (DF) and critical points (Sec. IV A), fundamental band-edge absorption (Sec. IV B), optical constants (Sec. IV C), and computational results on band structure and electronic transitions (Sec. IV D). Section V presents further discussions of the results as in Sec. V A a discrepancy between experimental and calculated optical response is discussed, in Sec. V B the dielectric function is decomposed into its interband contributions and the features are attributed to the electronic transitions, and in Sec V C the type of the critical points is used to confirm the location of the electronic transitions. A summary of the results (Sec. VI) concludes the paper.

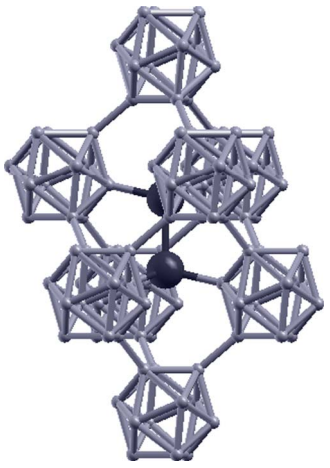

FIG. 1. (Color online) Rhombohedral unit cell of $B_{12}As_2$, generated with XCRYSDEN (Ref. 4) Body diagonal represents a threefold axis of symmetry and is known as trigonal axis (*c* axis here).

II. EXPERIMENTAL DETAILS

$B_{12}As_2$ films with a thickness of ~1.2 μm on 4H-SiC (0001) substrates were studied. They were prepared by chemical vapor deposition at a temperature of 1350 °C. Details of the growth can be found in Ref. 10. The $B_{12}As_2$ adopted the [111] growth orientation, as the film trigonal axis was parallel to $[0001]_{4H\text{-}SiC}$.[10] The optical response of the $B_{12}As_2$ was measured by spectroscopic ellipsometry recorded at room temperature in the energy range from 1.24 to 9.8 eV using both a Woollam VASE rotating compensator ellipsometer at multiple angles of incidence (Φ =55°,60°,65°,70°,75°) and a homemade synchrotron ellipsometer connected to BESSY II (Φ=68°).[11] To reduce substrate backside reflection in the ellipsometry measurements, an absorbing film was deposited onto the backside of the SiC substrate.

The measured ellipsometric parameters, Ψ and Δ, are related to the complex ratio ρ of the Frensel reflection coefficients, r_p and r_s, for light polarized parallel and perpendicular to the plane of incidence, respectively,

$$\rho = \frac{r_p}{r_s} = \tan \Psi e^{i\Delta}. \tag{1}$$

Under the assumption of an ideal single interface between vacuum and a surface and a semi-infinite material, the material complex DF could be derived by

$$\varepsilon = \sin^2 \Phi + \sin^2 \Phi \tan^2 \Phi \left(\frac{1-\rho}{1+\rho}\right)^2, \tag{2}$$

where Φ is the angle of incidence. However, for the thin film as studied here, a multilayered structure of substrate and film was considered, and a parameterized optical model was used to extract the complex dielectric function of $B_{12}As_2$ from the measured Ψ and Δ.[12] Surface roughness, experimentally quantified using atomic force microscopy, was included in the model using the effective-medium approximation[12] as 6 nm surface layer containing 50% voids. An abrupt interface between the $B_{12}As_2$ and SiC was assumed in the model for simplicity, neglecting a possible thin interfacial layer which has been reported for $B_{12}As_2$ growth on SiC.[13]

To determine CPs in the $B_{12}As_2$ DF, caused by Van Hove singularities in the joint density of states (DOS) of the band structure, the DF line shape was analyzed using the critical-point parabolic band (CPPB) model.[14] Within this model, the complex dielectric response $\varepsilon(\omega)$ is a superposition of oscillators (CPs),

$$\varepsilon_j(\hbar\omega) = A_j \exp(i\varphi_j)[\Gamma_j/(2\hbar\omega_j - 2\hbar\omega - i\Gamma_j)]^{n_j}$$
$$\text{for } n_j = \pm 0.5,\ 1$$

or

$$\varepsilon_j(\hbar\omega) = A_j \exp(i\varphi_j)\ln(2\hbar\omega_j - 2\hbar\omega - i\Gamma_j) \quad \text{for } n_j = 0, \tag{3}$$

where the parameters for jth CP are the amplitude A_j, energy $\hbar\omega_j$, broadening parameter Γ_j, phase projection factor φ_j, and dimensionality n_j of the CP that are closely related to the band structure. CP parameters were determined by analyzing the second derivative of the measured dielectric function after applying a Savitzky-Golay smoothing algorithm.[15] Dimensionality parameter n_j values of −0.5, 0, 0.5, and 1 correspond to three-dimensional (3D), two-dimensional (2D), one-dimensional (1D), and zero-dimensional (0D) (excitonic) critical points, respectively, dependent on in how many directions valence and conduction bands are parallel. The phase angle φ_j describes the type of the CP—maximum, minimum, or saddle point, as also the character of the excitonic effects.

III. COMPUTATIONAL METHOD

The band structure of icosahedral $B_{12}As_2$ was derived by noncollinear spin-orbit calculations, within the density-functional theory framework with the QUANTUM ESPRESSO code.[16] The plane-wave basis set for the electron wave functions was expanded up to a kinetic-energy cutoff of 37 Ry with periodic boundary conditions. Local-density approximation (LDA) functionals were used for the exchange correlation. For the boron atoms norm-conserving, nonrelativistic pseudopotential (PP) was used, generated with Perdew-Zunger (LDA) functional exchange correlation.[17] The 1s electrons were treated within the ionic core while 2s and 2p electrons were assigned to the valence band. For the arsenic atoms fully relativistic PP was employed that contained additional information for spin-orbit interaction and the valence electrons were considered to be of 4s and 4p orbitals. The norm-conserving PPs give a more accurate description of optical properties than ultrasoft PPs. The lattice parameters used in the calculations were as in Ref. 3; a_0=5.332 Å and α=70.52° of the rhombohedral structure with space group $R\bar{3}m$ (D_{3d} symmetry). The k point integrations over the Brillouin zone (BZ) were performed over a 6×6×6 Monkhorst and Pack mesh.

The first-principles dielectric function was determined from the band structure at the random-phase approximation (RPA) level.[18] Within this approach the imaginary part of the dielectric tensor $\varepsilon^j{}_2(\omega)$ is given by

$$\varepsilon_2^j(\omega) = \left(\frac{2\pi e}{m\omega}\right)^2 \sum_{v,c} \int_{\text{BZ}} d^3k |\langle vk| - i\hbar\partial_j |ck\rangle|^2 f_v^k (1 - f_c^k)$$
$$\times \delta(E_v^k - E_c^k - \hbar\omega), \tag{4}$$

where E_v and E_c are valence- and conduction-band eigenvalues, respectively, $\hbar\omega$ is the photon energy, the occupation numbers f_v=1 and f_c=0 are at zero temperature, and $|\langle vk| - i\hbar\partial_j|ck\rangle|$ is the dipole matrix element, j referring to the diagonal elements ε_{xx}, ε_{yy}, and ε_{zz} of the second-order tensor. A Drude-Lorentz broadening parameter of 0.2–0.3 eV helped to account for real material band broadening at room temperature. The real part of the dielectric function, $\varepsilon^j{}_1(\omega)$, was obtained from $\varepsilon^j{}_2(\omega)$ by the Kramers-Kronig relation.

IV. RESULTS

A. Complex dielectric function. High-energy critical points

Figure 2 shows the real $\varepsilon_1(\omega)$ and the imaginary $\varepsilon_2(\omega)$ parts of the dielectric function of $B_{12}As_2$ films as obtained by

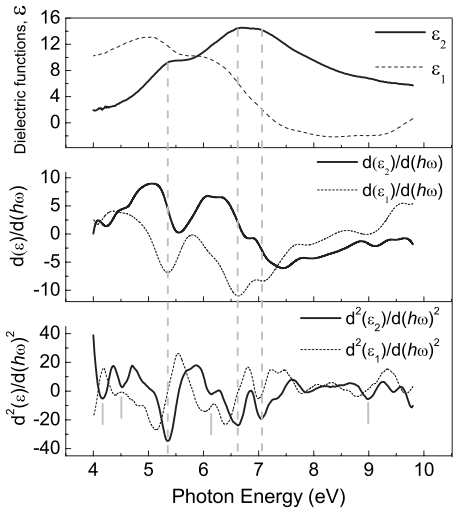

FIG. 2. Complex dielectric function of $B_{12}As_2$, its first and second derivatives.

spectroscopic ellipsometry in the spectral region between 4 and 9.8 eV. The $\varepsilon_2(\omega)$ dispersion shows pronounced features arising from CPs in the band structure. The numerically calculated first and second derivatives of the dielectric function are also presented in Fig. 2. CP parameters were obtained by simultaneously fitting of the second derivative of ε_2 and ε_1 of Eq. (3) to the experimental data second derivatives. The fitting result is illustrated in Fig. 3. The obtained CPs at 5.38, 6.62, and 7.04 eV are labeled E_0', E_1', and E_2, respectively. The energy position, dimensionality, and other oscillator parameters in Eq. (3), derived from the best fit, are given in Table I. There is also a shoulder in ε_2 at around 4–4.5 eV which, however, was not fitted as signal to noise was not high enough to obtain reliable enough second derivative data for this spectral range.

B. Fundamental band edge

Optical absorption of $B_{12}As_2$ was derived by fitting of the corresponding ellipsometry data, Ψ and Δ, for multiple angles of incidence as illustrated in Fig. 4. The absorption coefficient $\alpha=4\pi k/\lambda$ in the vicinity of the fundamental absorption edge is shown in Fig. 5(a). The optical absorption below the fundamental edge was exponentially dependent on the incident photon energy [Fig. 5(a), inset]. The broadening of $E_U=0.45$ eV was determined by fitting an Urbach tail to the experimental data. The large broadening might be due to the high density of states in the band gap established for the most of boron-rich solids. In the parabolic band-edge approximation, the absorption coefficient $\alpha(\hbar\omega)$ is given by $\alpha^n=A(\hbar\omega-E_t)$ for $\hbar\omega>E_t$,[19] where E_t is the transition energy, A a constant, $\hbar\omega$ photon energy, and the exponent n takes values of 2 and $\frac{1}{2}$ for allowed direct and indirect transitions, respectively, as presented in Figs. 5(b) and 5(c). The detailed energy of the lowest indirect transition taking place in $B_{12}As_2$ could not be determined by this approximation, as there is not a clear linear dependence in Fig. 5(b), which is also attributed to the presence of electronic states in the band gap. The absorption coefficient increases slightly above 3.5 eV while after 4 eV a much sharper rise took place [Fig. 5(a)]. Accordingly, a linear approximation of α^2 versus photon energy [Fig. 5(c)] determines the lowest direct band-gap energy of about 3.46 eV, which has only low probability and much stronger direct interband transitions at 3.9 eV.

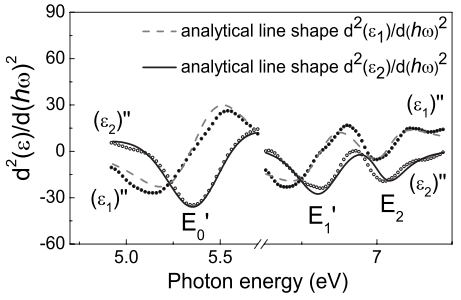

FIG. 3. Second derivatives with respect to the photon energy of the real and imaginary parts of the dielectric function $(\varepsilon_1)''$ and $(\varepsilon_2)''$ of $B_{12}As_2$ near the E_0', E_1', and E_2 critical points (dots). The best fit to the experimental data using Eq. (3) is also shown for $(\varepsilon_1)''$ with dashed gray line and for $(\varepsilon_2)''$ with black solid line.

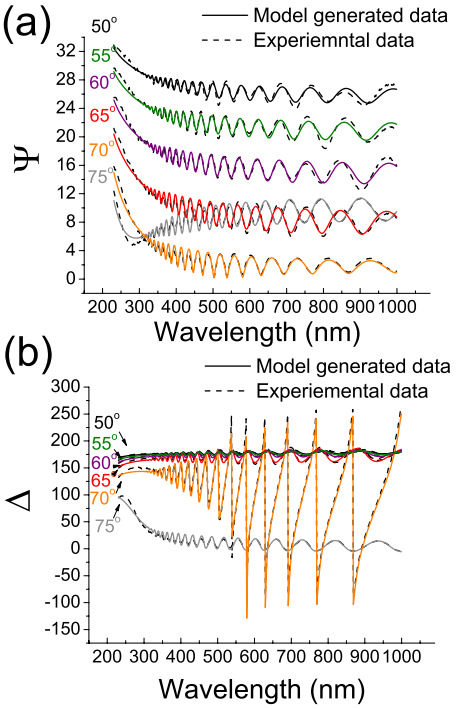

FIG. 4. (Color online) Experimental ellipsometry data, Ψ and Δ, and best fit to experimental data for $B_{12}As_2$/4H-SiC for angles of incidence from 50° to 75° (color online) in the spectral range from 230 to 1000 nm. The fringes here are the result of the finite film thickness of the $B_{12}As_2$, corresponding to a thickness of 1.239 μm.

C. Optical constants

Index of refraction and extinction coefficient of $B_{12}As_2$ below its band gap were also determined from the spectroscopic ellipsometry data. Figure 6 shows the complex refractive index of $B_{12}As_2$, i.e., index of refraction and extinction

TABLE I. Parameters of $B_{12}As_2$ CPs determined.

Label	E (eV)	Γ (eV)	φ	A (eV)	Dimensionality and type
E_0'	5.38	0.26	$3\pi/2$	2.52	1D M_0/0D (Fano line shape)
E_1'	6.62	0.31	$\pi/2$	4.1	2D M_1
E_2	7.04	0.18	0	1.7	3D M_1/2D M_0

coefficient for the region of normal dispersion. The index of refraction n of $B_{12}As_2$ is 2.7–2.8 for wavelengths between 550 and 1000 nm, increasing to 3.4 at 290 nm. The extinction coefficients k at 400–1000 nm is almost zero, as expected for below the band gap. Table II comprises the parameters of a Cauchy equation combined with Urbach absorption tail fitted to the experimental data to obtain the commonly used analytical description of optical parameters below a material band gap. To determine the long-wavelength dielectric constant $\varepsilon(\infty)$, the dispersion of the refractive index was fitted with the Sellmeier equation,[20] yielding $\varepsilon(\infty)=7.15$.

D. Computational results

Figure 7 illustrates the electronic band structure of $B_{12}As_2$ along the high-symmetry lines in the Brillouin zone, obtained by the first-principles calculations. The band dispersions are in good agreement with previous reports.[5–8] Relativistic corrections in electronic-structure calculation are important for materials with heavier elements such as As. For that reason we analyze the role played by spin-orbit relativistic effects. Figure 8 shows the band structures obtained from relativistic calculations [Fig. 8(a)] in comparison to nonrelativistic ones [Fig. 8(b)] for the band-edge states along Γ-A and Γ-Z principal axes of the BZ. The spin-orbit coupling results in a band splitting at the Γ point and along the Γ-Z direction, of states which are degenerate in the nonrelativistic description. The uppermost valence band was split by 1.58 meV at the Γ point and by $\sim$0.1 eV along the Γ-Z direction while the second highest valence band at Γ was also split by $\sim$0.1 eV. The lowest band gap with width of 2.56 eV is indirect from the twofold-degenerate valence-band maximum at $\Gamma(0,0,0)$ to the conduction-band minimum at $A(\frac{1}{2},0,0)$. The calculated total DOS is also shown in Fig. 7. The main contribution from different atomic orbitals was obtained from partial DOS calculations and the peaks in the total DOS are labeled accordingly. The main contribution to the upper valence bands are from the boron $2p$ and arsenic $4p$ orbitals. The lowest conduction band consists of arsenic $4p$ electrons, and also boron $2p$ electrons and arsenic $4d$-orbital electrons.

Effective masses of the carriers in $B_{12}As_2$ at Γ and along main directions in BZ were obtained from the band dispersion and are presented in Table III. Along $\langle 111\rangle$ the holes effective mass is lowest. Large hole effective masses, even an electronlike dispersion (negative effective mass) are obtained at the zone center Γ and along $\langle 100\rangle$ and $\langle 011\rangle$, hence there is a strong anisotropy in the hole effective mass. Electron effective mass is almost isotropic with the lowest value obtained along A-Γ $\langle 100\rangle$ (Table III).

A symmetry analysis of the electronic states was performed, considering they are spinors in the relativistic spin-orbit representation, and can be described by irreducible representations of the double point groups. $B_{12}As_2$ has inversion symmetry, so there are doubly degenerate states. Table IV gives the irreducible representations for the electronic wave functions at high-symmetry points for selected energy eigenvalues. The space group of the wavevector at zone center Γ is D_{3d}, as that of the $B_{12}As_2$ crystal. The group of the wave vector at high-symmetry point Z is D_{3d} while at A and B became C_{2h}. Table V shows the symmetry point group and irreducible representations for the wave functions along the axes connecting the high-symmetry points in the BZ.

To consider optical transitions in $B_{12}As_2$, the direct product of the symmetries of the ground and excited states must contain the irreducible representation corresponding to the dipole (x, y, and/or z) for a transition to occur. Allowed direct optical transitions from upper valence bands to the lower conduction bands at the high-symmetry points Γ, A, Z, B, and along Δ are schematically presented in Fig. 9. These are given for light polarized perpendicular to the $B_{12}As_2$ trigonal axis. The double point groups of the bands along high-symmetry axes are C_1, C_2, and C_s (Table V), i.e., optical transitions are also dipole allowed. The exception is the line Δ, connecting the Γ and Z points with symmetry of the double point group C_{3v}, where $\Gamma_5\rightarrow\Gamma_6$ and $\Gamma_6\rightarrow\Gamma_5$ transitions are symmetry forbidden (Fig. 9).

The RPA calculated real $\varepsilon_1(\omega)$ and imaginary $\varepsilon_2(\omega)$ dielectric functions of $B_{12}As_2$ are presented in Fig. 10, for

TABLE II. Cauchy-Urbach model (Ref. 20) fit parameters of the optical constants of $B_{12}As_2$ below the $B_{12}As_2$ band gap.

Dispersion type	Cauchy: $n(\lambda)=A+\frac{B}{\lambda^2}+\frac{C}{\lambda^4}$			Urbach: $k(\lambda)=Ae^{B(E-E_0)}$		
Parameter	A	B (μm^2)	C (μm^4)	A	B (eV^{-1})	E_0 (nm)
Value	2.69	0.023	0.0026	0.015	1.04	400

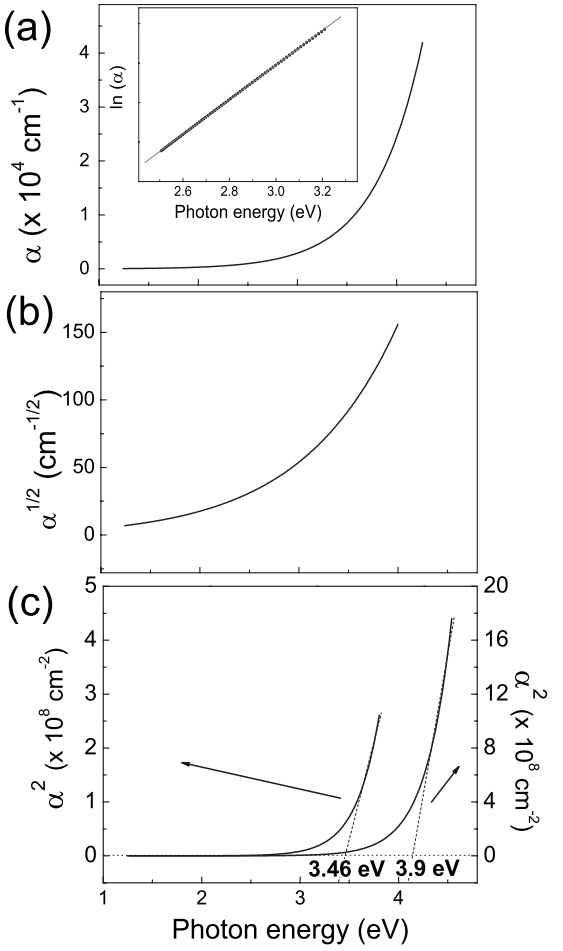

FIG. 5. (a) Absorption coefficient α as a function of phonon energy ($\hbar\omega$), (b) $\alpha^{1/2}$ vs $\hbar\omega$, and (c) α^2 vs $\hbar\omega$ in the vicinity of fundamental band edge. The inset in (a) shows the approximation of exponential Urbach tail. In (c) the dashed line is a linear approximation to the experimental data close to the direct interband transitions.

both, light polarized perpendicular ($E \perp c$) and parallel ($E \| c$) to the trigonal c axis. As expected for the rhombohedral lattice, crystalline $B_{12}As_2$ is optically uniaxial with the optical axis along the c axis. However, the obtained anisotropy $\Delta\varepsilon$ is

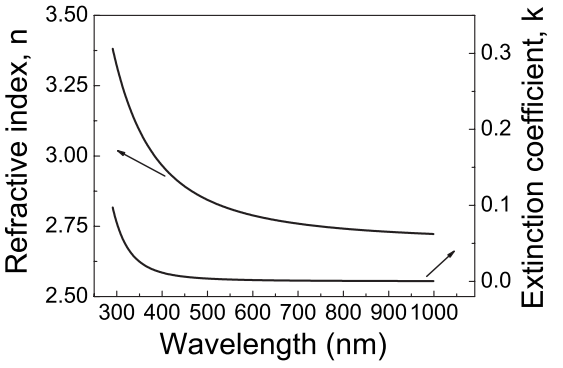

FIG. 6. Optical constants of $B_{12}As_2$, index of refraction and extinction coefficient, in the spectral range of normal dispersion from 290 to 1000 nm.

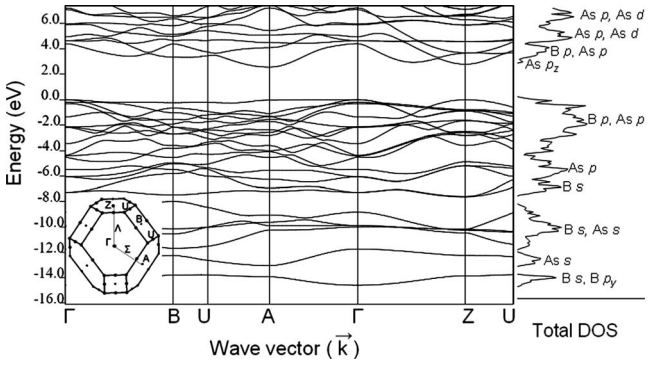

FIG. 7. Energy band dispersion of icosahedral $B_{12}As_2$ along symmetry lines in the Brillouin zone. Cartesian coordinates of the high-symmetry points in the Brillouin zone (inset, rhombohedral) are $B(0,\frac{1}{2},\frac{1}{2})$, U (0.60003, 0.39997, 0), $A(\frac{1}{2},0,0)$, $\Gamma(0,0,0)$, $Z(\frac{1}{2},\frac{1}{2},\frac{1}{2})$, and U (0.60003, 0.60003, 0.29995). Symmetries of the band states are presented in Table IV. Right panel is the calculated total density of states.

relatively small. This anisotropy was neglected in the experimental analysis of the ellipsometry data, which is here shown to be justified. The calculated first-principles static dielectric constant $\varepsilon_1(0)=\varepsilon_1(\omega=0)$ is 7.84 and 9.02 for $E \perp c$ and $E \| c$, respectively. The relation between the static dielectric constant $\varepsilon_1(0)$ and the long-wavelength dielectric constant $\varepsilon_1(\infty)$, determined from the optical dispersion below the band gap, should obey the Lyddane-Sachs-Teller relation[21] for polar material,

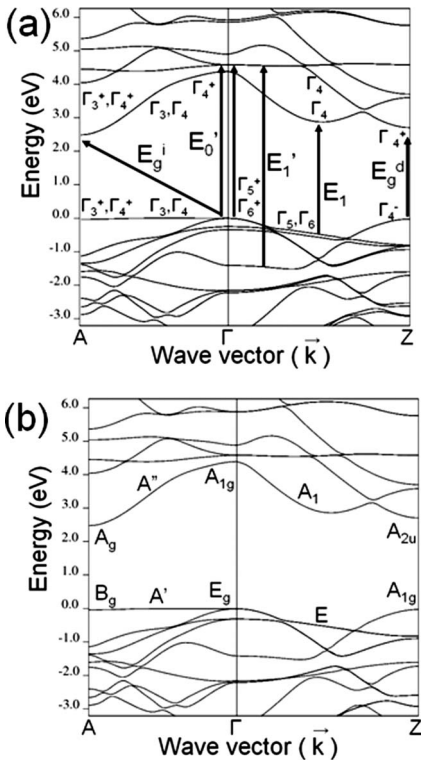

FIG. 8. Band-edge dispersion of $B_{12}As_2$ derived by (a) relativistic calculations and (b) nonrelativistic calculations. The main resolved electronic transition are indicated in (a) and are referred in the discussion section of the paper.

TABLE III. Calculated hole and electron effective masses m_h^* and m_e^* at valence-band maximum (heavy and light hole masses are m_{lh}^* and m_{lh}^*, respectively) and along ⟨111⟩, ⟨100⟩, and ⟨011⟩ directions (units of free-electron mass).

	m_h^*	m_e^*
Γ	$m_{lh}^*=0.46$, $m_{hh}^*=359$	
⟨111⟩	$0.49m_e$	$0.32m_e$
⟨100⟩	$7.00m_e$	$0.29m_e$
⟨011⟩	$3.69m_e$	$0.38m_e$

$$\frac{\varepsilon_1(0)}{\varepsilon_1(\infty)} = \left(\frac{\omega_L}{\omega_T}\right)^2, \tag{5}$$

where ω_L is the frequency of longitudinal optical phonons with zero wave vectors and ω_T is the frequency of transverse optical phonons with large wave vector. Substituting the experimental $\varepsilon_1(\infty)$ and calculated $\varepsilon_1(0)$ values for $E \perp c$ the ratio ω_L/ω_T that determines the electronic polarizability and the Reststrahlen band for $B_{12}As_2$ is 1.05.

V. DISCUSSION

A. Comparison of the experimental and calculated $\varepsilon_2(\omega)$

The imaginary part of the dielectric function $\varepsilon_2(\omega)$ is closely related to the joint density of states of the band structure, i.e., the possible optical transitions considering the density of available states in the both valance and conduction bands. As the normal to the surface of $B_{12}As_2$ films is parallel to the optical axis (trigonal axis) and taking into account that there is only a small anisotropy in the dielectric function (Fig. 10), the experimental configuration of the ellipsometry measurements used determines in good approximation the $E \perp c$ component of the dielectric function.[22] Figure 11(a) (top panel) shows the comparison of the corresponding imaginary part of the dielectric function $\varepsilon_2(\omega)$ determined from the *ab initio* band-structure calculation (Fig. 7) and the experimental data. This comparison of the experimental optical response with the theoretical dispersion shows good agreement. A broadening of 0.2–0.3 eV was assumed for the energy bands in determining the optical response function to consider natural linewidth broadening due to material imperfections and the finite temperature used in the measurements. An energy shift between the dielectric function dispersions from calculation and experiment is apparent, which is due the known underestimation of the energy band gap in the LDA first-principles calculations.[23]

B. Decomposition of $\varepsilon_2(\omega)$ into its interband contributions

To gain detailed insight into the origin of features in $\varepsilon_2(\omega)$ in terms of their origin in the band structure, a decomposition of $\varepsilon_2(\omega)$ into its band-to-band contributions was performed, with the main contributions illustrated in Fig. 11(a). Valence bands are enumerated v_1, v_2, v_3, v_4, and v_5, starting from the valence band top and conduction bands are c_1, c_2, c_3, c_4, and c_5, starting from the conduction-band minimum as indicated in Fig. 11(b), shown together with the vertical energy difference of the corresponding bands. Transitions, which mostly contribute to $\varepsilon_2(\omega)$, originate from parallel bands and band extremes between valence and conduction bands, also selection rules from symmetry considerations (Fig. 9) need to be taken into account.

Focusing on the lower photon energies range first, the optical absorption close to the band edge between 3 and 4 eV was due to band tails; the indirect transition should be at lower energy than the two determined direct interband transitions at 3.46 and 3.9 eV. In the calculated $\varepsilon_2(\omega)$ only direct

TABLE IV. Point group, energy, degeneracy, irreducible representations, and occupation ($f_v=1$ and $f_c=0$ at zero temperature) of the selected electronic band states at Γ, Z, A, B, and U point of the $B_{12}As_2$ BZ.

Electronic band states	Energy (eV)	Degeneracy	Irreducible representation	Occupation
Γ point (D_{3d})	4.961	2	Γ_5^-,Γ_6^-	1
	5.732	1	Γ_4^+	1
	6.781	1	Γ_4^+	1
	6.872	2	Γ_5^+,Γ_6^+	1
	7.090	1	Γ_4^+	1
	7.092	2	Γ_5^+,Γ_6^+	1
	11.506	1	Γ_4^+	0
	11.740	1	Γ_4^+	0
	11.741	2	Γ_5^+,Γ_6^+	0
	12.040	1	Γ_4^-	0
	12.990	1	Γ_4^-	0
	13.054	2	Γ_5^-,Γ_6^-	0
Z point (D_{3d})	5.46	1	Γ_4^-	1
	6.180	1	Γ_4^+	1
	6.230	1	Γ_4^-	1
	6.287	2	Γ_5^-,Γ_6^-	1
	6.289	2	Γ_5^+,Γ_6^+	1
	7.088	1	Γ_4^-	1
	9.882	1	Γ_4^+	0
	10.747	1	Γ_4^+	0
	10.749	1	Γ_4^+	0
	11.666	1	Γ_4^+	0
	11.667	2	Γ_5^+,Γ_6^+	0
	12.973	1	Γ_4^+	0
	12.979	2	Γ_5^+,Γ_6^+	0
A point (C_{2h})	5.538	2	Γ_3^+,Γ_4^+	1
	5.744	2	Γ_3^-,Γ_4^-	1
	5.783	2	Γ_3^-,Γ_4^-	1
	5.997	2	Γ_3^+,Γ_4^+	1
	7.058	2	Γ_3^+,Γ_4^+	1
	9.652	2	Γ_3^+,Γ_4^+	0
	11.188	2	Γ_3^+,Γ_4^+	0
	11.586	2	Γ_3^+,Γ_4^+	0
	12.198	2	Γ_3^+,Γ_4^+	0
	12.542	2	Γ_3^-,Γ_4^-	0

TABLE IV. (*Continued.*)

Electronic band states	Energy (eV)	Degeneracy	Irreducible representation	Occupation
B point (C_{2h})	4.939	2	Γ_3^+,Γ_4^+	1
	5.183	2	Γ_3^-,Γ_4^-	1
	5.550	2	Γ_3^-,Γ_4^-	1
	6.062	2	Γ_3^+,Γ_4^+	1
	6.421	2	Γ_3^-,Γ_4^-	1
	6.849	2	Γ_3^+,Γ_4^+	1
	10.446	2	Γ_3^+,Γ_4^+	0
	11.480	2	Γ_3^-,Γ_4^-	0
	11.755	2	Γ_3^+,Γ_4^+	0
	12.088	2	Γ_3^+,Γ_4^+	0
	12.243	2	Γ_3^+,Γ_4^+	0
U point (C_2)	4.665	2	Γ_3,Γ_4	1
	4.717	2	Γ_3,Γ_4	1
	5.161	2	Γ_3,Γ_4	1
	5.243	2	Γ_3,Γ_4	1
	5.330	2	Γ_3,Γ_4	1
	5.780	2	Γ_3,Γ_4	1
	6.011	2	Γ_3,Γ_4	1
	6.081	2	Γ_3,Γ_4	1
	6.496	2	Γ_3,Γ_4	1
	10.791	2	Γ_3,Γ_4	0
	10.959	2	Γ_3,Γ_4	0
	11.644	2	Γ_3,Γ_4	0
	11.769	2	Γ_3,Γ_4	0
	11.864	2	Γ_3,Γ_4	0
	12.773	2	Γ_3,Γ_4	0

transitions were considered. The lowest vertical transition at A point of the BZ of 2.59 eV is dipole forbidden (Fig. 9) while for the direct transition at Z with energy of 2.79 eV the value of the dipole matrix element is small, hence the oscillator strength for this transition is low, making only a small contribution to the $\varepsilon_2(\omega)$. The first pronounced peak in the calculated dielectric function comes from the direct transition at 3.3 eV. The analysis shows that this transition takes place between v1 and c1 bands at the extreme along ⟨111⟩ (Γ-Z) in Fig. 11(b). The experimentally obtained direct optical band gap found at 3.9 eV in Fig. 5(c) can be assigned to this transition, as it is the first direct transition with high oscillator strength [E_1 in Fig. 8(a)]. According to the calculations the valence bands along Γ-Z are split, thus a split-off peak $E_1+\Delta$ with $\Delta=0.1$ eV is possible, however it was not detected at room temperature. The discrepancy between the experimental and theoretical transition energy of ~0.6 eV is due to the known self-energy problem of the LDA calculations, leading to underestimate of the band gap by 50–100 %.[23] Then, assuming LDA correction of about ~0.6 eV, the first low strength direct transition, observed experimentally at about 3.46 eV corresponds to the 2.79 eV direct transition at Z point of the BZ [E_g^d in Fig. 8(a)].

TABLE V. Point group and irreducible representations of states along main symmetry axes in the BZ of $B_{12}As_2$.

High-symmetry direction	Point group	Irreducible representations of all bands
Δ (Γ-A), ⟨100⟩	C_s	Γ_3,Γ_4
Λ (Γ-Z), ⟨111⟩	C_{3v}	$(\Gamma_4;\Gamma_5;\Gamma_6)$
Σ (Γ-B), ⟨011⟩	C_s	Γ_3,Γ_4
B-U	C_2	Γ_3,Γ_4
U-A	C_1	Γ_2
Z-U	C_s	Γ_3,Γ_4

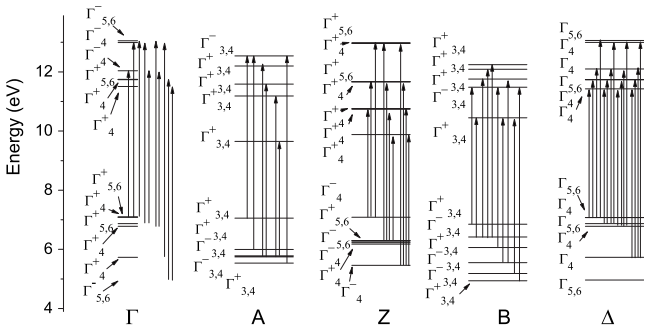

FIG. 9. Symmetry allowed optical transitions between $B_{12}As_2$ electronic states for light polarized perpendicular ($E\perp c$) to the film c axis at Γ, A, Z, and B point, and along Γ-Z (Δ). The U point is omitted, as all transitions are allowed, as there are no symmetry forbidden transitions in its point group (C_2).

If we revert to the fundamental band edge, the band calculations show that it is $E_g^i=2.56$ eV, between the valence-band maximum at the Γ point and the conduction-band minimum at the A point of the BZ. This theoretical result is in agreement with the plane-wave-based calculations by Morrison *et al.*,[8] who determined an indirect band gap of 2.609 eV. Armstrong *et al.*[7] reported $E_g^i=2.3$ eV while the calculations performed by Li and Ching,[5] based on orthogonalized linear combination of atomic orbitals and LDA, showed $E_g^i=2.78$ eV, taking place from the valence band at the Z point to the conduction band at the A point. Experimentally [Fig.

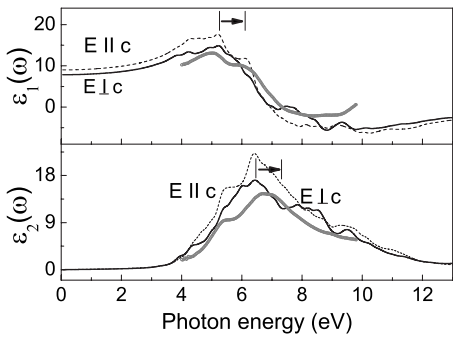

FIG. 10. Calculated real and imaginary parts of dielectric function $\varepsilon_1(\omega)$ and $\varepsilon_2(\omega)$, respectively, for light polarized perpendicular ($E\perp c$, solid) and parallel ($E\|c$, dashed) to the c axis of $B_{12}As_2$. Experimental points are also presented in gray. The arrows indicate that the calculated dielectric response should be shifted due to the self-energy correction of the band gap.

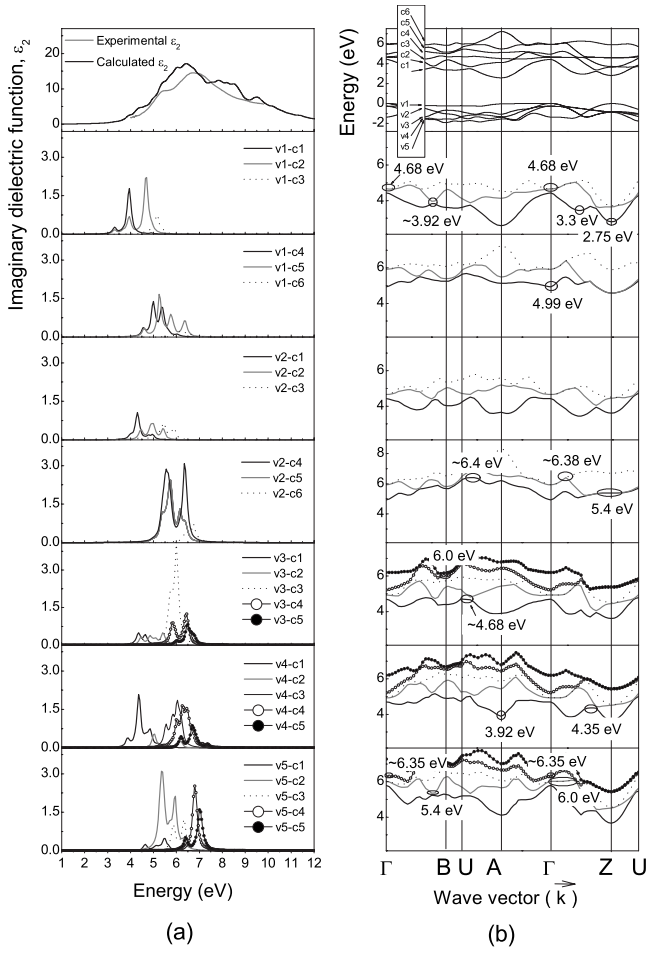

FIG. 11. (a) Calculated imaginary part of dielectric function $\varepsilon_2(\omega)$ of $B_{12}As_2$ for $E \perp c$ and its decomposition into band-to-band contribution. Top panel of (a): calculated $\varepsilon_2(\omega)$ broadened by 0.2–0.3 eV is also shown and its comparison to experimentally determined $\varepsilon_2(\omega)$. (b) The vertical energy differences of individual bands from (a) and at top panel of (b)—the band diagram close to the band gap.

5(b)] it was not possible to unambiguously identify the presence of an indirect band gap and its energy. Nevertheless, considering a ~0.6 eV LDA correction consistent with our results discussed before and also later, the indirect band-gap energy E_g^i can be estimated from the first-principles calculations to be about 3.2 eV. This value is 0.27 eV lower than the only experimental value of the $B_{12}As_2$ band gap reported by Slack *et al.*[9] on bulk $B_{12}As_2$ material from optical-absorption spectra. However, the discrepancy could be because the absorption spectrum in the vicinity of the fundamental edge strongly depends on the crystalline quality.

Next, we focus on the high-energy critical points to verify our absorption edge results. The experimental data show three distinct features at 5.38 (E_0'), 6.62 (E_1'), and 7.04 eV (E_2) (Table I), and furthermore features around 4–4.5 eV (Fig. 2). Compared to the calculations and considering the LDA energies underestimation, we can therefore conclude that features around 5.38–7.04 eV in the experimentally measured $\varepsilon_2(\omega)$ possibly arise from transitions related to the 4.68, 6.0, and 6.38 eV peaks in the calculated dielectric function in Fig. 11, although these different contributions could not be precisely separated in the experiment due to linewidth broadening. The theoretical analysis of the decomposed $\varepsilon_2(\omega)$ shows that the peak at 4.68 eV arises from transitions from v1 to c2 close to the zone center Γ where both bands are approximately parallel along Γ-Z, Γ-A, and Γ-B, with further contributions from transitions between the parallel bands v3 and c1 along U-A. Note that though the electronic transitions between v1 and c2 are dipole forbidden at the zone center, they are dipole allowed along the high-symmetry axes. These transitions, in particular, those related to v1-c2 can provide the origin for the CP at 5.38 eV determined experimentally [Fig. 8(a)]. As they occur close to the zone center, the labeling E_0' is used here in consistency with the convention in Ref. 24. The assignment is also consistent with the LDA correction assumed before, as for this CP the experimental energy is 0.7 eV higher than the LDA estimate for this transition.

At higher photon energies the experimentally determined CP at 6.62 eV can be attributed to the 6.0 eV high intensity peak in the theoretical dispersion [Fig. 11(b)]. Decomposition of $\varepsilon_2(\omega)$ shows that the latter has contributions from transitions between v5 and c2, along Γ-Z, where the bands are strongly parallel, thus justifying the high intensity of this transition in the experiment. As this transition occurs along the Γ-Z direction ($\langle 111 \rangle$), hence it could be labeled E_1' in accordance with the convention in Ref. 24 and it is also depicted in Fig. 8(a). The nature of the CP at 7.04 eV (E_2) is more complicated, as it is associated with the broad 6.38–6.5 eV peak in calculated $\varepsilon_2(\omega)$, having various parallel contributions. The theoretical analysis of this high intensity peak [Fig. 11(b)] shows contributions from transitions between v2-c4 along U-A, v2-c5 transition along Γ-Z, and v5-c3 transitions close to Γ and along Γ-B, with further other small contributions.

Except the above discussed pronounced CPs, there are also other minima in the second derivative of the experimental $\varepsilon_2(\omega)$ (Fig. 2), the assignment of which could further support the conclusions from the analysis. The observed feature at 4.5 eV when corrected with the 0.6 eV for LDA self-energy could be well accounted by the 3.92 eV transition in the calculations, originating from the first allowed transitions at A point, between v4 and c1 [Fig. 11(b)], with contribution along the six equivalent $\langle 110 \rangle$ (Γ-B) directions. The kink in the experimental $\varepsilon_2(\omega)$ at about 5 eV could originate from the calculated transition of 4.35 eV, with its primary contribution from v4-c1 at the small region of parallel bands along Γ-Z. The feature at 6.1 eV, which is subsequent to the E_0' CP, could be well accounted to the 5.38 eV theoretical peak, due to parallel bands transitions v2-c4 in the vicinity of Z point, and v5-c2 transitions along Γ-B. Above 7 eV the integral intensity of $\varepsilon_2(\omega)$ starts decreasing with no distinct further features in the dielectric function for the energy range investigated here.

C. Type of the critical points in $\varepsilon_2(\omega)$

To further confirm and identify in more detail the assignment of transitions to the CPs, the dimensionality of CPs can

TABLE VI. Optical transitions in $B_{12}As_2$: experimental energy, first-principles theoretical energy, and corresponding wave vector location of the transition in BZ.

Optical response feature—label	Energy experiment (eV)	Energy[a] theory (eV)	Initial and excited state bands	Interband transition
E_g^i	3.2	2.56	v1-c1	$\Gamma \rightarrow A$
E_g^d	3.46	2.79	v1-c1	Z
E_1	3.90	3.30	v1-c1	Γ-Z
E_0'	5.38	4.68	v1-c2	Γ-Z, Γ-A and Γ-B, U-A
E_1'	6.62	6.00	v5-c2	2D Γ-Z ⟨111⟩
E_2	7.04	6.38–6.5		Different contributions:
			v2-c4	flat region along U-A
			v2-c5	flat region along Γ-B at Γ
			v5-c3	extreme along Γ-Z

[a]Self-energy gap correction of about 0.6–0.7 eV should be considered when comparing the theoretical energies with the experimental ones.

be considered as given in Table I, determined by fitting Eq. (3) to the experimental data (Fig. 3). The critical point E_0' at 5.38 eV is fitted best with a 1D M_0 line shape ($n=0.5$, $\varphi=3\pi/2$), corresponding to a one-dimensional minimum. As discussed, interband transitions in the vicinity of the zone center Γ along high-symmetry axes ⟨111⟩, ⟨100⟩, and ⟨011⟩ corresponding in the calculation to a peak in $\varepsilon_2(\omega)$ at 4.68 eV can be considered, assuming a self-energy gap correction of ~0.6–0.7 eV. This interband transition is from the uppermost valence band (v1) to the second conduction band (c2), for which the valence and conduction bands are mostly parallel along the main BZ symmetry lines, consistent with the dimensionality of this critical point determined. We note that the line shape of the experimentally measured CP could also be fitted reasonably well with 0D excitonic line shape ($n=1$, $\varphi \approx \pi$), corresponding to a Fano resonance, i.e., an interfering discrete energy states and a continuum of states in which case transitions in the vicinity of the BZ center along Γ-Z, Γ-A, and Γ-B and along U-A could be considered.

For the E_1' CP at 6.62 eV, the best fit to the experimental data was produced using a 2D M_1 CP (Table I), corresponding to a two-dimensional maximum. The counterparting feature in the calculated $\varepsilon_2(\omega)$ at about 6 eV (Fig. 11), in particular, the v5 and c2 bands that are strongly parallel along ⟨111⟩ in the BZ, is consistent with this type of CP. The CP E_2 at 7.04 eV is a broader feature, containing contributions from different regions of the BZ. This peak was fitted within the CPPB model using a line shape of a 3D M_1 saddle point and a 2D M_0 critical point, although since this CP consists of various contributions, this fitting was used to determine a CP energy rather than the nature of CP. From the calculation as discussed before the corresponding feature in the calculated $\varepsilon_2(\omega)$ at 6.38 eV (Fig. 11) contains many contributions which cannot be separated here in the experimental data. Table VI summarizes the assignments of dominant optical transitions to the different experimentally determined CPs.

VI. CONCLUSIONS

The complex dielectric function of icosahedral $B_{12}As_2$ was obtained from 1.24 to 9.8 eV. Analysis of the dielectric function in terms of the critical-point parabolic band model was performed. High-energy critical points were assigned to interband transitions by comparing the experimental data to theoretical first-principles calculations based on plane-wave basis sets and LDA exchange-correlation functionals. The theoretical dielectric function was in good agreement with the experimental response function when a self-energy LDA correction of 0.6 eV was assumed. This finding enabled to establish the fundamental band gap, low- and high-energy interband transitions, and to identify their origin in the Brillouin zone. An experimental value for the static dielectric constant and theoretical values for holes and electrons effective mass of $B_{12}As_2$ were also determined.

ACKNOWLEDGMENTS

This research was supported by the Engineering and Physical Science Research Council (Grant No. EP/D075033/1), by the National Science Foundation Materials World Network Program (Grants No. 0602875 and No. 0602807 under the NSF-EPSRC Joint Materials Program), and by the European Community through the "NanoCharM" project under the Seventh Framework Programme (FP7). We acknowledge the Helmholtz-Zentrum Berlin-Electron storage ring BESSY II for provision of synchrotron radiation at beamline3m-NIM-A and would like to thank M. Roppischer for assitance. The research leading to these results has received funding from the European Community's Seventh Framework Progreamme (FP7/2007–2013) under grant agreement No. 226716.

[1] H. Chen, G. Wang, M. Dudley, Z. Xu, J. H. Edgar, T. Batten, M. Kuball, L. Zhang, and Y. Zhu, Appl. Phys. Lett. **92**, 231917 (2008).
[2] Y. Gong, M. Tapajna, Y. Zhang, M. Dudley, Y. Zhang, J. H. Edgar, M. Hopkins, M. Kuball, L. Zhang, and Y. Zhu, Appl. Phys. Lett.(unpublished).
[3] C. Beckel, N. Lu, B. Abbott, and M. Yousaf, Inorg. Chim. Acta **289**, 198 (1999).
[4] A. Kokalj, Comput. Mater. Sci. **28**, 155 (2003).
[5] D. Li and W. Y. Ching, Phys. Rev. B **52**, 17073 (1995).
[6] F. Gao, X. Qin, L. Wang, Y. He, G. Sun, Li Hou, and W. Wang, J. Phys. Chem. B **109**, 14892 (2005).
[7] D. R. Armstrong, J. Bolland, and P. G. Perkins, Theor. Chim. Acta **64**, 501 (1984).
[8] I. Morrison, D. M. Bylander, and L. Kleinman, Phys. Rev. B **45**, 1533 (1992).
[9] G. A. Slack, T. M. McNelly, and E. A. Taft, J. Phys. Chem. Solids **44**, 1009 (1983).
[10] R. Nagarajan, Z. Xu, J. H. Edgar, F. Baig, J. Chaudhuri, Z. Rek, E. A. Payzant, H. M. Meyer, J. Pomeroy, and M. Kuball, J. Cryst. Growth **273**, 431 (2005).
[11] C. Cobet, R. Goldhahn, W. Richter, and N. Esser, Phys. Status Solidi B **246**, 1440 (2009).
[12] R. M. A. Azzam and M. Bashara, *Ellipsometry and Polarized Light* (North-Holland, Amsterdam, 1987).
[13] J. R. Michael, T. L. Aselage, D. Emin, and P. G. Kotula, J. Mater. Res. **20**, 3004 (2005).
[14] D. E. Aspnes, *Handbook on Semiconductors* (North-Holland, Amsterdam, 1980), Vol. 2.
[15] A. Savitzky and M. J. Golay, Anal. Chem. **36**, 1627 (1964).
[16] P. Giannozzi, Stefano Baroni, Nicola Bonini, Matteo Calandra, Roberto Car, Carlo Cavazzoni, Davide Ceresoli, Guido L. Chiarotti, Matteo Cococcioni, Ismaila Dabo, Andrea Dal Corso, Stefano de Gironcoli, Stefano Fabris, Guido Fratesi, Ralph Gebauer, Uwe Gerstmann, Christos Gougoussis, Anton Kokalj, Michele Lazzeri, Layla Martin-Samos, Nicola Marzari, Francesco Mauri, Riccardo Mazzarello, Stefano Paolini, Alfredo Pasquarello, Lorenzo Paulatto, Carlo Sbraccia, Sandro Scandolo, Gabriele Sclauzero, Ari P. Seitsonen, Alexander Smogunov, Paolo Umari, and Renata M. Wentzcovitch, J. Phys.: Condens. Matter **21**, 395502 (2009); http://www.quantum-espresso.org
[17] G. B. Bachelet, D. R. Hamann, and M. Schlüter, Phys. Rev. B **26**, 4199 (1982).
[18] H. Ehrenreich and M. H. Cohen, Phys. Rev. **115**, 786 (1959).
[19] J. I. Pankove, *Optical Processes in Semiconductors* (Dover, New York, 1975).
[20] Jai Singh, *Optical Properties of Condensed Matter and Applications* (Wiley, New York, 2006).
[21] K. Shirai and S. Gonda, J. Phys. Chem. Solids **57**, 109 (1996).
[22] G. E. Jellison, Jr. and J. S. Baba, J. Opt. Soc. Am. A Opt. Image Sci. Vis. **23**, 468 (2006).
[23] R. M. Martin, *Electronic Structure: Basic Theory and Practical Methods* (Cambridge University Press, Cambridge, England, 2004).
[24] P. Y. Yu and M. Cardona, *Fundamentals of Semiconductors: Physics and Materials Properties* (Springer, New York, 2005).